A COMPUTATIONAL STUDY ON DROPLET IMPINGEMENT ONTO A THIN LIQUID FILM

Saeed Asadi*

Department of Mechanical Engineering
Khorasan Institute of Food Science and Technology (KRIFST)
Khorasan Science and Technology Park
Mashhad, Iran

Mohammad Passandideh-Fard

Department of Mechanical Engineering
Ferdowsi University of Mashhad
Mashhad, Iran

الخلاصة:

تمّت دراسة عمليّة ارتطام قُطيرة على غشاء سائل رقيق بوساطة إجراء مُحاكاة حسابيّة. وقد تمّ حلّ مُعادلات Navier-Stokes للسوائل غير الثابتة، والمائعة اللاضَغوطة، واللـّزجة في نِظام الإحداثيّات المُتماثل المحاور بوساطة طريقة التحكّم في الحجم. وتمّ استعمال أسلوب حجم السائل (VOF) لتتبّع سطح السائل الحُرّ. وقد أظهرت نتائج الأنموذج توافقاً جيّداً مع القياسات المِخبريّة. ووُجد أنّ العمليّات الديناميكيّة بعد الارتطام سريعة التأثر بسرعة القـُطيرة الابتدائيّة وعمق حوض السائل. وتم حساب التطوير الزمني لعُلوّ التاج وقِطره بوساطة المُحاكاة الحسابيّة. وتمّ أيضاً حساب عُلوّ التاج الأقصى وزمنه المُناظر على أعداد ويبر (We) مختلفة وعلى سماكات مختلفة للغشاء. وأظهرت النتائج أن السماكة اللابعدية للغشاء السائل لها تـأثيرٌ ضـئيل على العوامل اللابعديـة المُتعلّقـة بعُلـوّ التـاج الأقصـى وزمنـه المُنـاظر. ومن ثـمّ تمّـت دراسـة العـدد We الحـرج للـرشّ (We_{cr}) علـى أعـداد Oh (Ohnesorge) مختلفة ضمن النطاق 0.1~0.01؛ وأظهرت النتائج توافقاً جيّداً مع نتائج الاختبارات. وأُجريَت المحاكاة الحسابيّة أيضاً لأعداد Oh أقل (Oh~0.001) وحيث لا يمكن إجراء التجارب بسبب الحدود المفروضة من الأجهزة. ووُجد أن عدد We الحرج عديم التـأثر بسماكة الغشاء اللابعديّة؛ إلا أنّه ينقُصُ مع تناقص العدد Oh أو لزوجة السائل. وأخيراً، تمّ وضع مُعادلات بسيطة تربط ما بين العوامل اللابعديّة المُختلفة والمُهمّة في عمليّة ارتطام القـُطيرة على غشاء سائل رقيق.

* Corresponding author:
E-mail: asadi@krifst.ir , asadi@kstp.ir , asadiinfo@yahoo.com

Paper Received August 13, 2008; Paper Rewritten March 14, 2009; Paper Accepted March 27, 2009

ABSTRACT

The impingement of a droplet onto a thin liquid film is studied by numerical simulation. The Navier–Stokes equations for unsteady, incompressible, viscous fluids in the axisymmetric coordinate system are solved using a control volume method. The volume-of-fluid (VOF) technique is used to track the free-surface of the liquid. Model predictions are in good agreement with experimental measurements. It is found that the dynamic processes after impact are sensitive to the initial droplet velocity and the liquid pool depth. The time evolution of the crown height and diameter are obtained by numerical simulation. The maximum crown height and its corresponding time are calculated using the model for different We (Weber) numbers and various film thicknesses. Results show that the non-dimensional film thickness has a small effect on the non-dimensional parameters related to the maximum crown height and its corresponding time. Next, the critical We number for splashing (We_{cr}) is studied for Oh (Ohnesorge) numbers in the range of 0.01~0.1; the results compare well with those of the experiments. The numerical simulation is also performed for lower Oh (Oh~0.001) where experiments cannot be performed due to limitations in the instruments. The critical We number is found to be insensitive to the non-dimensional film thickness; it decreases, however, with decreasing Oh number or liquid viscosity. Finally, simple expressions are developed that correlate the non-dimensional parameters involved in the droplet impingement onto a thin liquid film.

Key words: droplet impingement, free surface flows, liquid crown, numerical simulation, thin liquid film

Nomenclature:

D_0	initial droplet diameter
f	liquid volume fraction
$\vec{F}_b$	body force per unit volume
$\vec{F}_{ST}$	surface tension force
g	gravitational constant
$\vec{g}$	gravitational acceleration
H	crown height
H^*	non-dimensional crown height
$H^*_{\max}$	maximum non-dimensional crown height
h	liquid film thickness
h^*	dimensionless film thickness
k	total curvature of the interface
$\hat{n}$	unit normal vector
Oh	Ohnesorge number
P	pressure
R^2	coefficient of determination
S	area of free surface
t	time
t^*	non-dimensional time
$t^*_{\max}$	maximum non-dimensional time
$\vec{V}$	velocity vector
V_0	droplet velocity before impact
We	Weber number
We_{cr}	critical impact Weber number
δ	Dirac delta function
$\vec{x}$, $\vec{y}$	position vectors
Δt	time step
γ	liquid-gas surface tension
μ	dynamic viscosity
ρ	density
$\tilde{\tau}$	shear stress tensor
Ω	volume
∇	del operator

Subscripts and Superscripts

i, j, k	mesh indices
n, n+1	time levels
o	initial
s	free surface
'	interim
*	non-dimensional

A COMPUTATIONAL STUDY ON DROPLET IMPINGEMENT ONTO A THIN LIQUID FILM

1. INTRODUCTION

Droplet impingement onto a thin liquid film is a phenomenon relevant to many technical applications such as spray cooling, spray painting, corrosion of turbine blades, and fuel injection in internal combustion engines. It is also discussed in many natural phenomena such as the erosion of soil and the dispersal of spores and micro-organisms. When a drop impacts vertically on a liquid film, an axisymmetric liquid sheet (crown) grows up and, depending on the impinging drop size and velocity and liquid characteristics (like viscosity, density, and surface tension), liquid jets may protrude from the crown and subsequently break up to form secondary droplets (Figure 1). The fluid mechanics of droplet collision on a solid surface has been studied with great detail in the literature [1–4]. Not many studies, however, have considered the collision of a droplet onto a liquid film. The recent progress in the field of drop and spray impact on a wetted wall can be attributed to the rapid development of experimental techniques, allowing one to obtain high-quality images of impacting drops and to collect detailed information about the splashing threshold, drop shape, crown propagation, fingering of the rim, *etc.* [5–8].

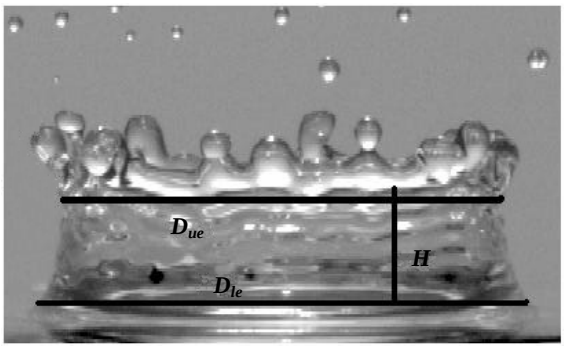

Figure 1. Splash process and morphology: D_{ue} is crown upper external diameter, D_{le} crown lower external diameter, H crown height

There exists a considerable literature describing numerical models of droplet impact on a solid surface. Harlow and Shannon [9] were the first to simulate this phenomenon. They used a ‘‘marker-and-cell’’ (MAC) finite-difference method to solve the fluid mass and momentum conservation equations, while neglecting the effect of viscosity and surface tension to simplify the problem. Trapaga and Szekely [10] applied a commercial code, FLOW-3D [11], that uses the Volume-of-Fluid (VOF) method, to study the impact of molten particles. Liu *et al.* [12] employed another VOF based code, RIPPLE [13], to simulate molten metal droplet impact. Pasandideh-Fard *et al.* [14] applied a modified SOLA-VOF [15] method to model the impact of water droplets in which varying amounts of a surfactant were dissolved to modify the liquid-solid contact angle. Adaptive-grid finite element methods were used by Fukai *et al.* [16] to simulate water droplet impact on a flat surface. In their study, the initial rate of change of the splat height was found to be directly proportional to the droplet impact velocity. Furthermore, the maximum splat radius decreased with the value of the dynamic contact angle for the spreading stage. The effect of impact velocity on droplet spreading was more pronounced when the wetting was limited. Bussmann *et al.* [17] published a description of a three-dimensional, finite-volume, fixed-grid Eulerian model they developed, which used a volume-tracking algorithm to locate the droplet free surface during its impact on a solid surface. They simulated water droplets falling with low velocity (~ 1 m/s) onto either an inclined plane or the edge of a step, and compared model predictions with photographs of impacting droplets. Their paper discussed ways of specifying boundary conditions at the liquid–solid contact line, the effect of which is especially important during droplet recoil following impact when fluid flow is dominated by surface tension forces. Pasandideh-Fard *et al.* [1] extended the three-dimensional model of Bussmann *et al.* [17] to include heat transfer and solidification. They combined a fixed-grid control volume discretization of the fluid flow and energy equations with a volume-tracking algorithm to track the droplet free surface and an improved fixed velocity method to track the solidification front. Surface tension was modeled as a volume force acting on fluid near the free surface. To validate the model, their simulated depositions of tin droplets onto both horizontal and inclined stainless steel surfaces were compared to those of the experiments. The agreement between the two results was good both qualitatively and quantitatively.

Considerably fewer computational studies have been performed on droplet collision onto liquid films. Josserand and Zelaski [18] proposed a theory predicting the transition between splashing and deposition for impacting droplets

on a thin liquid film that was supported by numerical simulation. They employed a potential flow model everywhere except in the small neck region of the developed crown. The effects of viscosity and surface tension on the crown formation were discussed. Their discretization in numerical solution was performed on a Marker and Cell (MAC) grid and the pressure was solved by the explicit projection method. The interface was followed by the VOF method and Piecewise Linear Interface Calculation (PLIC); the capillary force was computed through a variant of the Continuum Surface Stress (CSS) and Continuum Surface Force (CSF) methods. The results presented, however, are more focused on the jet formation at the early stages of the droplet impact on the liquid film. Xie *et al.* [19] studied the process of a single liquid drop impact onto a thin liquid film with a numerical simulation using the moving particle semi-implicit (MPS) method. They validated their model by a comparison with experiments. They found that the dynamic process after impact was sensitive to the thickness of the liquid pool and the initial drop velocity. When the initial drop velocity was low, the drop merged with the liquid film and no strong splash was observed. The numerical results provided, however, show that the particle method does not provide an accurate prediction of the sharp liquid-gas interface, especially when the liquid film becomes thin and it breaks up into small droplets.

In this study, the impingement of a droplet onto a thin liquid film is numerically simulated using a modified VOF technique based on the more accurate technique of Youngs' algorithm in an axisymmetric coordinate system. The results of the model are compared with those of the experiments available in the literature. The effects of important processing parameters on the dynamic process of the impingement are studied. Simulations are also performed on very small Oh (Ohnesorge) numbers in the order of 0.001, for which no measurements are reported due to the limitations existing in the experiments.

2. NUMERICAL METHOD

2.1. Governing Equations

A schematic of a droplet impingement onto a liquid film is shown in Figure 2. The mathematical description of the problem is formulated subject to these assumptions:

(i) the droplet is spherical prior to impact, (ii) the liquid is incompressible and Newtonian, (iii) the liquid density, viscosity and surface tension are constant, (iv) the flow during the impact is laminar [1,17,20], (v) a single velocity characterizes fluid motion prior to the impact (which precludes considering an internal circulation of the fluid within the droplet prior to the impact), and (vi) the influence of the surrounding gas on the liquid during the impact is negligible (which implies that viscous stresses at the free surface are assumed to be zero).

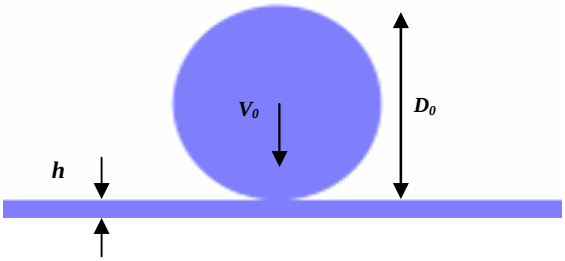

Figure 2. A schematic of a droplet impingement onto a liquid film. D_o is drop diameter, V_o drop velocity before impact and h liquid film thickness

The equations of conservation of mass and momentum in the liquid may then be written as [1,17]:

$$\nabla \cdot \vec{V} = 0 \tag{1}$$

$$\frac{\partial \vec{V}}{\partial t} + \nabla \cdot (\vec{V}\vec{V}) = -\frac{1}{\rho}\nabla P + \frac{1}{\rho}\nabla \cdot \tilde{\tau} + \vec{g} + \frac{1}{\rho}\vec{F}_b \tag{2}$$

where $\vec{V}$ represents the velocity vector, P the pressure, ρ the liquid density, $\tilde{\tau}$ the shear stress tensor, $\vec{g}$ the gravitational acceleration, and $\vec{F}_b$ any body forces (per unit volume) acting on the fluid.

The flow equations have been written in an Eulerian frame of reference, and thus a solution of these equations must be coupled with some methodology for following the deforming liquid-gas interface. The VOF technique is applied to track the time evolution of the liquid free surface. A color function, *f*, is introduced to represent the volume fraction of liquid in a computational cell. If the control volume is filled with liquid alone, the color function is unity. When only air exists in the control volume, *f* takes on a value of zero. When both liquid and gas are present, the color function value lies between zero and one. The advection of function *f* is governed by [1,17]:

$$\frac{\partial f}{\partial t} + (\vec{V} \cdot \nabla) f = 0 \tag{3}$$

The volume force, $\vec{F}_b$, appearing in Equation (2), consists of the gravitational force and the surface tension force which is given as [21]

$$\vec{F}_{ST}(x) = \gamma \int_s k(\vec{y}) \hat{n}(\vec{y}) \, \delta(\vec{x} - \vec{y}) \, dS \tag{4}$$

by means of the CSF model. In this equation, $\hat{n}$ represents a unit vector normal to the interface directed into the liquid, γ represents the liquid-gas surface tension, k the total curvature of the interface, δ is the Dirac delta function, and $\vec{x}$ and $\vec{y}$ are position vectors. The integration is performed over some area of free surface S. k and $\hat{n}$ are geometric characteristics of the surface, and may be written in terms of f:

$$k = -\nabla . \hat{n} \quad , \quad \hat{n} = \frac{\nabla f}{|\nabla f|} \tag{5}$$

Expressed as a body force, surface tension is then incorporated into Equation (2) via the term $\vec{F}_b$. To reduce the size of the computational domain, symmetric boundaries are applied when possible. Along a symmetric boundary, fluid velocity obeys slip and no penetration conditions. Boundary conditions are also imposed at the liquid free surface, denoted by subscript s. The boundary condition on velocity is the zero shear stress condition:

$$\tau_s = 0 \tag{6}$$

and since the surface tension force has been included in Equation (2), the boundary condition on pressure reduces to:

$$p_s = 0 \tag{7}$$

A boundary condition for f is unnecessary since f is a Lagrangian invariant. The initial condition for f is defined by specifying a droplet diameter D_o. Fluid velocity within the droplet is characterized by a single impact velocity and the initial pressure within the droplet is defined by the Laplace equation:

$$\vec{V} = \vec{V}_0 \quad , \quad P_0 = 4\frac{\gamma}{D_0} \tag{8}$$

2.2. Numerical Procedure

Figure 3 illustrates a typical mesh where velocities are specified at the center of cell faces and pressure at each cell center. Equations (1) and (2) are solved with a two-step projection method, in which a forward Euler time discretization of the momentum equation is divided into two steps:

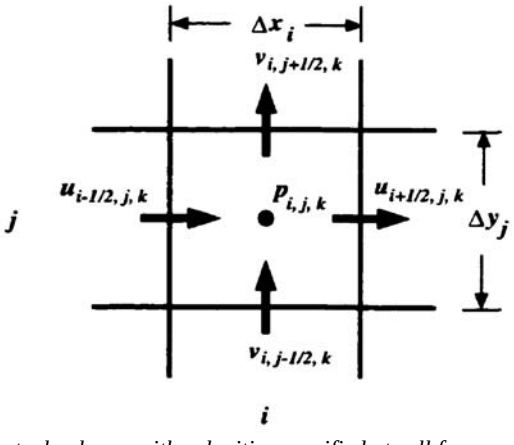

Figure 3. A 2D control volume, with velocities specified at cell faces, pressure at the cell center

$$\frac{\vec{V}' - \vec{V}^n}{\Delta t} = -\nabla \cdot (\vec{V}\vec{V})^n + \frac{1}{\rho}\nabla \cdot \tilde{\tau}^n + \vec{g}^n + \frac{1}{\rho}\vec{F}_b^n \tag{9}$$

$$\frac{\vec{V}^{n+1} - \vec{V}'}{\Delta t} = -\frac{1}{\rho^n}\nabla P^{n+1} \tag{10}$$

In the first step, using Equation (9), an interim velocity $\vec{V}'$ is computed explicitly from convective, viscous, gravitational, and body force accelerations of the known field $\vec{V}^n$ for a timestep Δt. In the second step, using

Equation (10), $\vec{V}^n$ is projected onto a divergence-free velocity field. Combining Equation (10) with Equation (1) at the new time level *(n+1)* yields a Poisson equation for pressure:

$$\nabla \cdot (\frac{1}{\rho^n} \nabla P^{n+1}) = \frac{1}{\Delta t} \nabla \cdot \vec{V}' \tag{11}$$

The RHS of Equation (9) is discretized according to the conventions typical of the finite volume method**.** Integrating Equation (9) over a control volume $\Omega_{i,j}$ yields:

$$\frac{1}{\Delta t}\int_{\Omega_{i,j}} (\vec{V}' - \vec{V}^n) d\Omega = -\int_{\Omega_{i,j}} \nabla \cdot (\vec{V}\vec{V})^n d\Omega + \frac{1}{\rho}\int_{\Omega_{i,j}} \nabla \cdot \vec{\tau}^n d\Omega + \int_{\Omega_{i,j}} \vec{g}^n d\Omega + \frac{1}{\rho}\int_{\Omega_{i,j}} \vec{F}_b^n d\Omega \tag{12}$$

Applying Gauss' theorem to convert the first two volume integrals on the RHS to integrals over the control volume surface $S_{i,j}$ and assuming that the other integrands are constant throughout $\Omega_{i,j}$, Equation (12) becomes

$$\frac{\vec{V}' - \vec{V}^n}{\Delta t} = -\frac{1}{\Omega_{i,j}}\int_{S_{i,j}} \vec{V}^n (\vec{V}^n \cdot \hat{n}_S) dS + \frac{1}{\rho \Omega_{i,j}}\int_{S_{i,j}} (\vec{\tau}^n \cdot \hat{n}_S)\, dS + \vec{g}^n + \frac{1}{\rho}\vec{F}_b^n \tag{13}$$

where $\hat{n}_S$ is the unit outward normal to $S_{i,j}$.

The following algorithm advances the solution by one timestep. Given velocity, pressure, and volume fraction fields at the time level *n* [1]:

1. evaluate $\vec{V}'$ using Equation (9)
2. solve Equation (11) implicitly for P^{n+1}**,** incorporating boundary conditions on *P*
3. evaluate $\vec{V}^{n+1}$ using Equation (10)
4. apply boundary conditions on $\vec{V}^{n+1}$
5. evaluate a new fluid volume distribution f^{n+1} using Equation (3) and obtain the new shape of liquid-gas free surface using Youngs' algorithm [22]
6. reapply boundary conditions on $\vec{V}^{n+1}$

Repetition of these steps allowed advancing the solution through an arbitrary time interval. The computational domain encompassed the initial droplet and sufficient volume for the liquid film to cover the liquid deformation and subsequent crown formation during the impingement. The mesh size was determined on the basis of a mesh refinement study in which the grid spacing was progressively decreased until further reductions made no significant changes in the predicted crown shape during the impact. The droplet was discretized using a computational mesh, with a uniform grid spacing equal to 1/40 of the droplet radius. Numerical computations were performed on a Pentium 4 computer. Typical CPU times ranged from three to six hours.

3. RESULTS AND DISCUSSION

The first case considered is that of the collision of a single droplet impinging vertically onto a liquid film with D_o=4.2 mm, V_o=5.098 m/s, and h=2.1 mm where D_o is droplet diameter, V_o droplet velocity before impact and h liquid film thickness. Experimental results for this case are available in the literature. Wang and Chen [7] developed a novel technique for studying droplet impact on very thin films of liquid. In their experiment, the glycerol-water solutions were used as the working medium, and the impacting droplet and target liquid were of the same fluid. Viscosity of their solutions was 0.01~0.06 Pa.s which is much higher compared to that of water (*i.e.* 0.001 Pa. s). These viscous solutions were used to form a very thin liquid film with a uniform thickness. The 'single-shot-flash' photographic technique was used to freeze the instantaneous motion of the impact, and the impinging velocity was measured from the images of the droplet during the last 0.1 ms period before it contacts the target liquid film. They presented their results for three cases with different values for the film thickness and impact velocity.

Figure 4 compares images calculated using numerical model with photographs given by Wang and Chen [7] for a case where the density (ρ) of the glycerol–water solution was 1200 kg/m^3, the viscosity (μ) 0.022 Ns/m^2 (Pa.s), and the surface tension (γ) 0.0652 N/m. Therefore, the Ohnesorge number (Oh=$\mu/(\gamma\rho D_0)^{0.5}$) for this case is 0.0384. As observed from Figure 4, there is a good qualitative agreement between calculated images (3D views and cross sections) and experimental photographs. The formation of corona seen in photographs is well predicted by the numerical model. The time of each image (t), measured from the instant of first contact with the liquid film, is also indicated in the figure. Both simulations and experiments show that after droplet impact, a conical rebound jet is formed that propagates radially outward, forming a thin cylindrical liquid film called corona. The corona reaches its maximum height at t=10 ms, after which it starts to subside into the liquid film.

To further study the impact dynamics of this case, the pressure distribution in the liquid film and droplet is shown in Figure 5. The pressure at the time of impact is suddenly increased to a high pressure right at the impact point. The high pressure region extends radially in the liquid as the droplet spreads over the surface and pushes the liquid film outwards. The pressure at the center (impact point) has the maximum value and gradually decreases in the radial direction. After the formation of the corona, the pressure drops considerably, as shown in Figure 5 at t=0.5 ms. At the end of the process, when the corona subsides in the surrounding liquid layer, the pressure everywhere is decreased to the reference pressure, which is assumed to be zero in the simulation. Figure 5 also shows the velocity distribution and streamlines on a cross section of the droplet and liquid film during the impact process. The velocity of the droplet at the time of impact is decreased to a low velocity in the liquid film and increased to a high velocity in the jet formation zone. After the formation of the corona, the velocity remains higher in the corona zone relative to the other domain. This continues to the end of the process when the corona subsides in the surrounding liquid film.

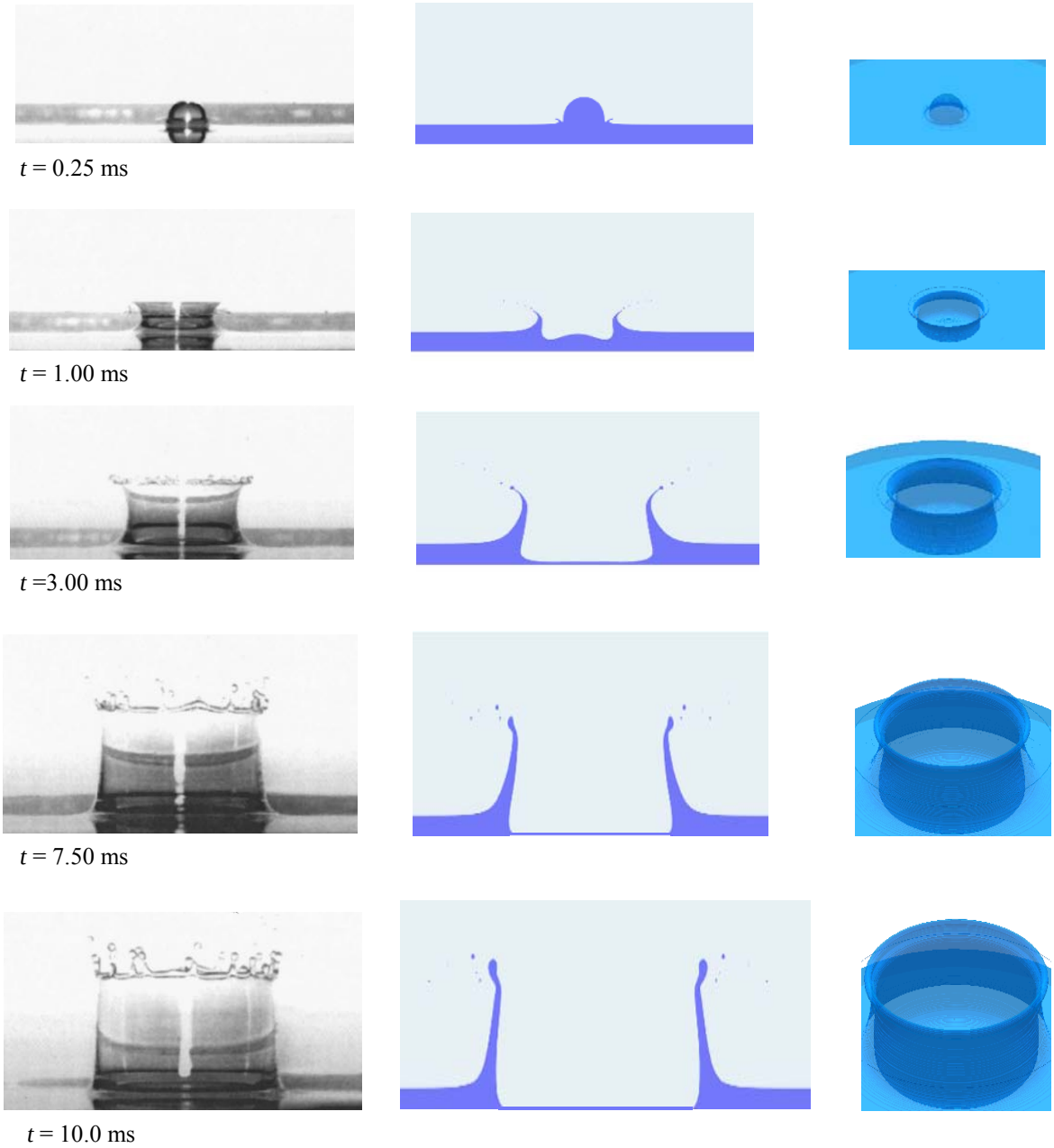

Figure 4. Computer generated images (3D view and cross-section) and photographs [7] of a 4.2 mm diameter droplet impacting with a velocity of 5.098 m/s onto a liquid film with a thickness of 2.1 mm

To present a quantitative comparison between the results of the model with those of the experiments, the measured data reported by Wang and Chen [7] and Cossali *et al.* [8] are used. The distance between the crown base and the rim is termed the crown height H (see Figure 1). Dividing this height by the initial droplet diameter results in the non-dimensional crown height denoted by H^* ($=H/D_o$). The crown height evolution was investigated in the experiments of Cossali *et al.* [8] by analyzing the images taken from the side. They measured the non-dimensional

crown height versus non-dimensional time ($t^*=V_o t/D_o$) for all of their experimental conditions. The results of their experiments are shown in Figures 6–8 where the measured variation of H^* versus t^* is plotted along with the model predictions for the same conditions. The droplet diameter and velocity were held constant such that the We number ($We=\rho V_o^2 D_o/\gamma$) was 667. The liquid film thickness, however, was changed. Normalizing this thickness by the droplet diameter results in a dimensionless film thickness

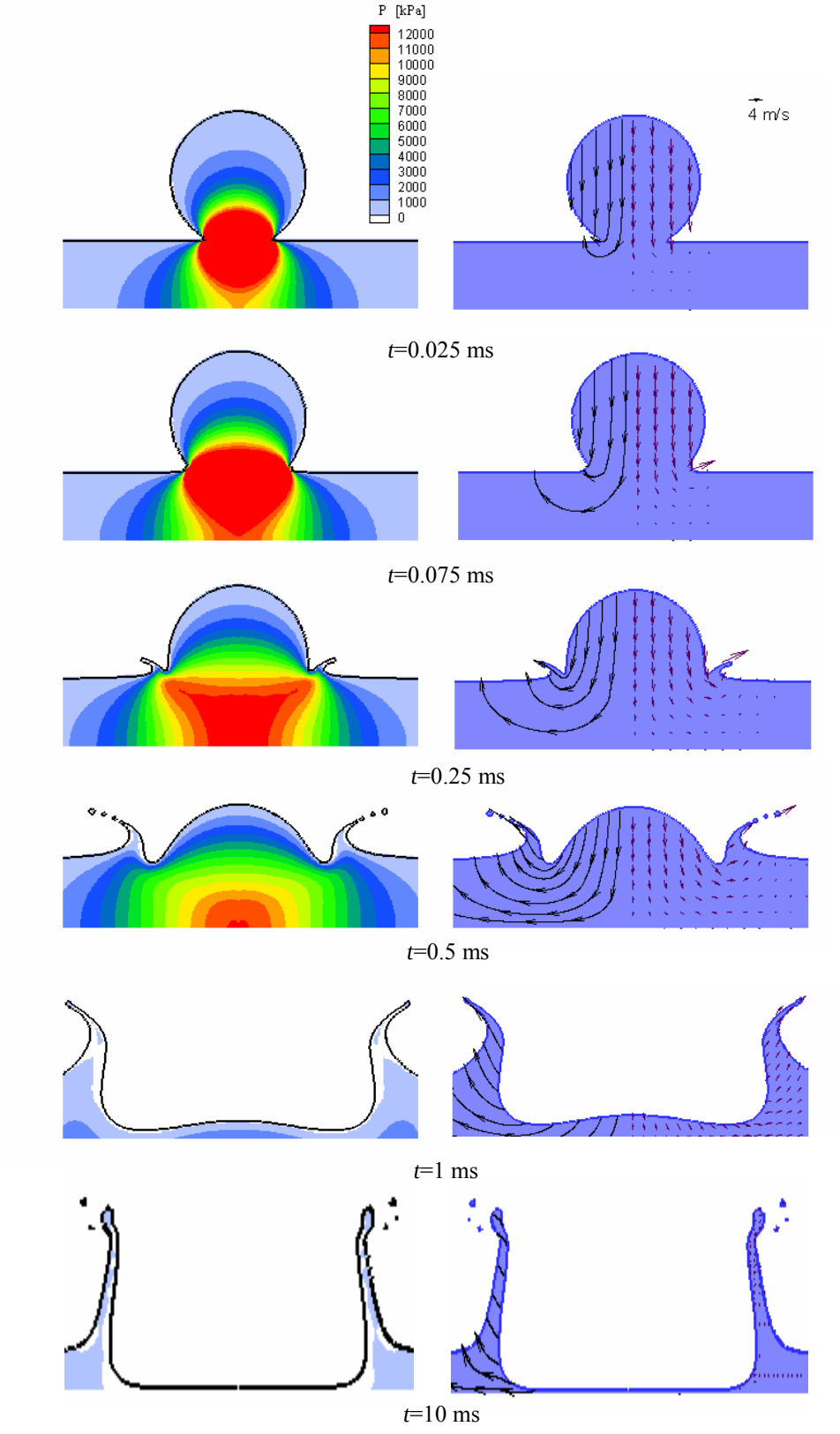

Figure 5. The pressure and velocity distributions in the droplet and liquid film. Droplet diameter is 4.2 mm, impacting velocity 5.098 m/s and liquid film thickness 2.1 mm. Streamlines are also shown in the figure.

denoted by $h^*(=h/D_o)$. For Figures 6–8, the value of h^* was 0.29, 0.67, and 1.13, respectively. A good quantitative agreement between the model predictions with those of the experiments validates the model and its underlying assumptions.

The definition of "crown diameter" hides some uncertainties. In fact, as can be observed in Figure 1, the crown is not usually cylindrical, and the diameter of the external surface varies with the distance from the surface of the film. To account for this uncertainty, two diameters were defined when analyzing the pictures taken from the side: the upper external diameter (D_{ue} measured at the base of the rim) and the lower external diameter (D_{le} measured at the crown base), as seen in Figure 1. Figure 9 shows the time evolution of the two crown diameters from numerical simulations and experiments for the impact of a water droplet with We=667 onto a liquid film with a thickness corresponding to h^*=0.67. The elapsed time shown in the figure is measured from the moment of impact.

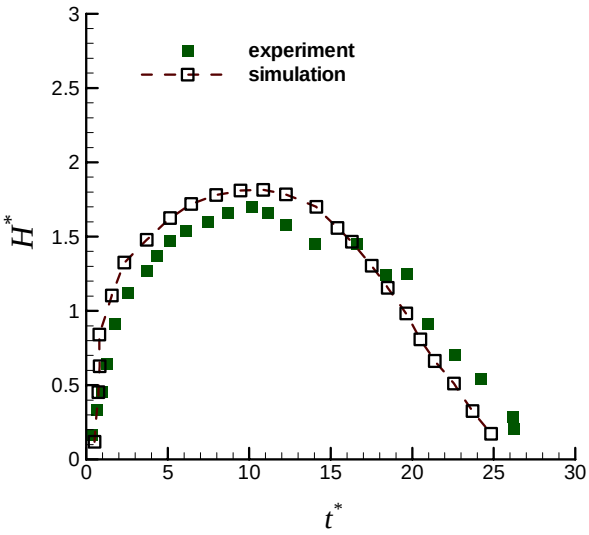

Figure 6. A comparison between numerical and experimental [8] results for the evolution of non-dimensional crown height for a case with We=667 and a non-dimensional liquid film thickness of h^*=0.29

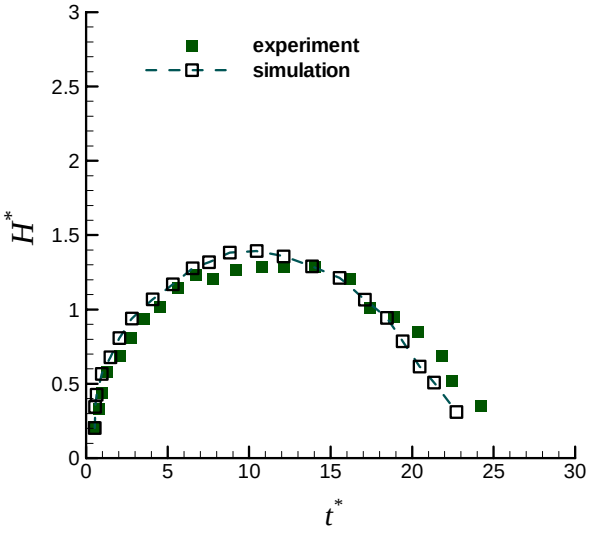

Figure 7. A comparison between numerical and experimental [8] results for the evolution of non-dimensional crown height for a case with We=667 and h^*=0.67

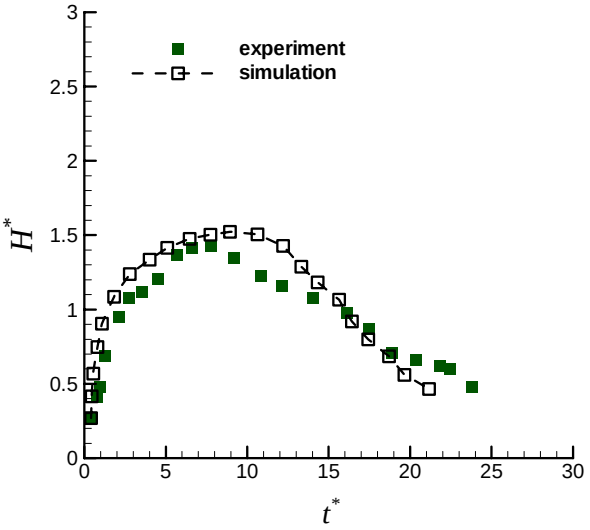

Figure 8. A comparison between numerical and experimental [8] results for the evolution of non-dimensional crown height for a case with We=667 and h^*=1.13

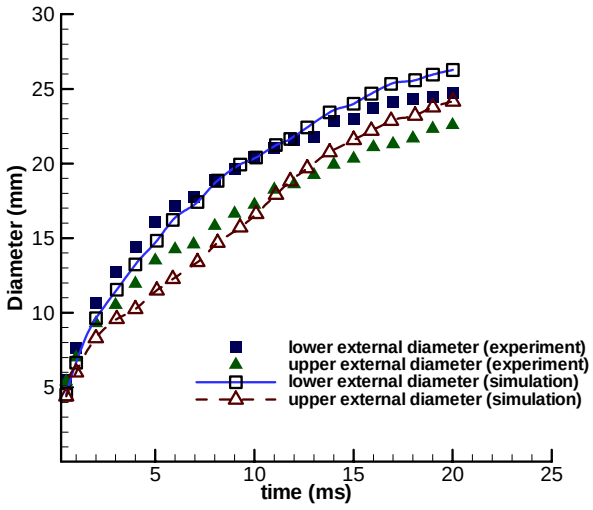

Figure 9. A comparison between numerical and experimental [8] results for time evolution of the "crown diameters" for a case with We=667 and h^*=0.67

The crown height reaches a maximum value ($H^*_{\max}$) after a certain time ($t^*_{\max}$) from the impact. These two non-dimensional values were calculated from the results of the numerical model for various film thicknesses. Figure 10 shows the variation of the non-dimensional maximum crown height ($H^*_{\max}$) against the non-dimensional film thickness (h^*) for the impact We numbers ranged from 296 to 1020. It can be seen from this figure that $H^*_{\max}$ is mainly influenced by We and less by h^*; therefore, $H^*_{\max}$ can be expressed in terms of We. Using the concept of curve fitting, the following equation could be obtained from the figure:

$$H^*_{\max} = 0.0025\,We \tag{14}$$

The maximum and minimum errors associated with Equation (14) are presented in Table 1. The coefficient of determination (R^2) for these error calculations is also provided in the same table. The R^2 coefficient is a statistical measure that shows how well the regression equation approximates the real data points; an R^2 of 1.0 indicates a perfect fit of data. The most general definition of the coefficient of determination is:

$$R^2 = 1 - \frac{\sum_i (a_i - b_i)^2}{\sum_i (a_i - \bar{a})^2} \tag{15}$$

A data set has values a_i each of which has an associated modeled value b_i. Here, a_i is the observed value, b_i is the predicted value by the regression equation, and $\bar{a}$ is the average value of a_i. $\sum_i (a_i - \bar{a})^2$ represents the total sum of squares (proportional to the sample variance) and $\sum_i (a_i - b_i)^2$ is the sum of squared errors also called the residual sum of squares.

As seen from the table, a value of 0.92 for R^2 indicates an accurate data fitting by Equation (14). The variation of the maximum non-dimensional time ($t^*_{\max}$) against the non-dimensional film thickness (h^*) is shown in Figure 11 for the same We numbers as of those for Figure 10. Similarly, from this figure, it is seen that $t^*_{\max}$ is only a function of We, whereby curve fitting is expressible as:

$$t^*_{\max} = 0.0037\,We^{1.2} \tag{16}$$

The maximum and minimum errors for this equation along with the corresponding coefficient of determination (R^2) are also presented in Table 1. The R^2 for this equation is 0.946, indicating the accuracy of Equation (16) on fitting the data points.

In the experiments of Wang and Chen [7], the critical impact We number (We_{cr}) for splashing was determined as a function of the non-dimensional film thickness. Splashing was defined as those impacts where secondary droplets were ejected from the crown upon impact. Figure 12 shows the results of both numerical simulation and experiments for the variation of We_{cr} with h^* for three different fluids (60%, 70%, and 80% glycerol-water solution) in the range of h^*<0.1. As observed in Figure 12, the numerical results are in good agreement with those of the experiments. The critical impact We number for splashing was found to be independent of film thickness. Impact with the 80% glycerol-water solution was found to have the highest critical impact We number equal to 800. The 60% and 70% glycerol-water solution resulted in critical impact We numbers of 400 and 500, respectively. Differences in the critical impact We number for the different glycerol-water solutions were believed to be due to differences in the liquid viscosity.

In the Wang and Chen novel technique [7], viscous fluids {Oh (0.1–.01)} were used because of equipment limitations in generating a thin liquid film. As a result, they could not set up their experimental system for a low-viscous liquid-like water. This is why values for critical impact We numbers in the range of practical Oh numbers (around 0.001) were not reported. Water droplets with a diameter of 2–4.4 mm have Oh equal to 0.00262–0.0018. Predicted critical We numbers from numerical simulation for such droplets impacting onto a very thin water film are also displayed in Figure 12 where h^*<0.1 and Oh ranged from 0.00262 to 0.0018. Figure 12 shows that We_{cr} is only affected by Oh number; therefore, similar to the last two expressions, a correlation can be obtained by curve fitting as:

$$We_{cr} = 790\,(1 - e^{-24\,Oh}) \tag{17}$$

Similar to the previous two curve fitting equations, the coefficients of determination for Equation (17) was calculated. The results along with the maximum and minimum errors are given in Table 1.

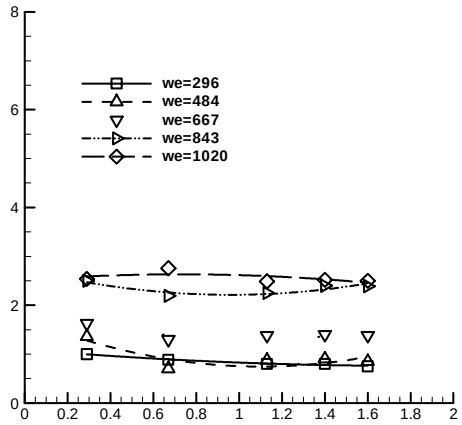

Figure 10. The variation of the maximum non-dimensional crown height ($H^*_{\max}$) against non-dimensional liquid film thickness (h^*) for different We numbers ranged from 296 to1020

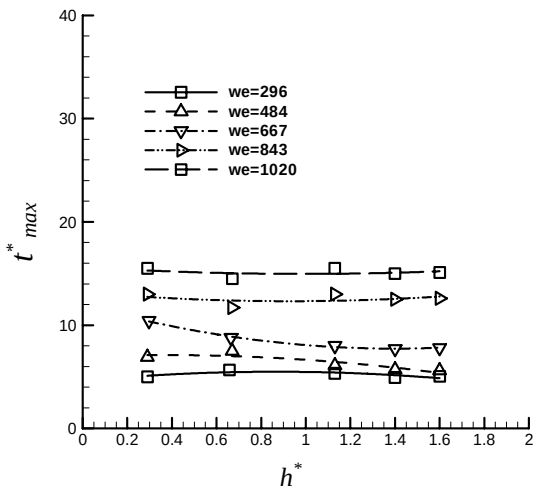

Figure 11. The variation of t^*_{max} against non-dimensional film thickness (h^*) for different We numbers ranged from 296 to1020

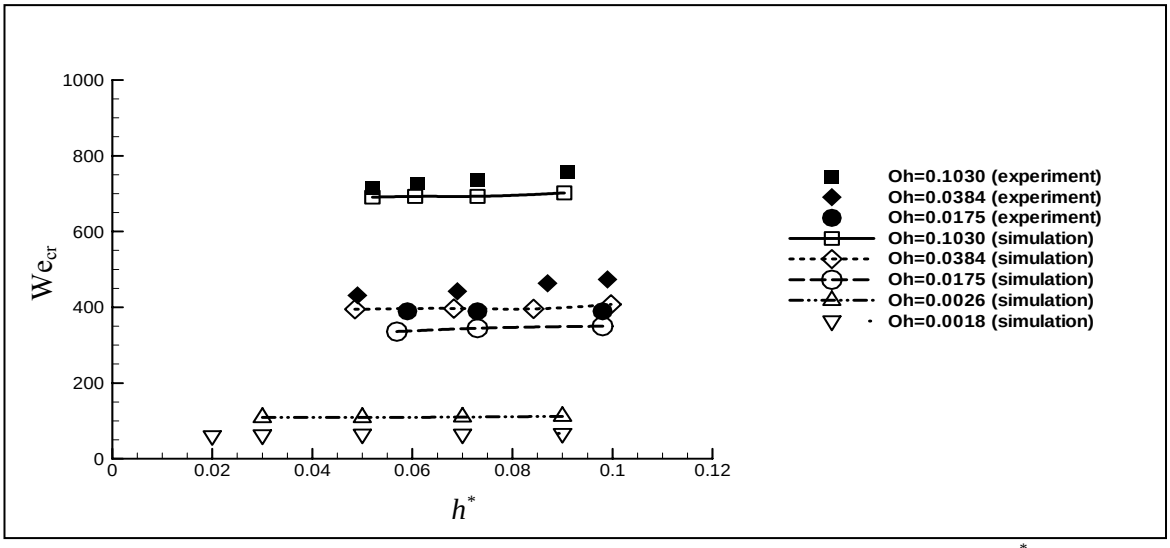

Figure 12. A comparison between numerical and experimental [7] results for the variations of We_{cr} against h^* for three different fluids (60%, 70%,and 80% glycerol-water solution) in the range of h^*<0.1 and Oh ranged from 0.0175 to 0. 0.1030. The figure also shows the predicted critical We number from numerical simulation for lower Oh numbers equal to 0.00262 and 0.0018 where no measurements are reported in the literature.

4. CONCLUSIONS

The collision dynamics of droplet impingement onto a thin liquid film were studied by means of computer simulations. The Navier–Stokes equations for unsteady, incompressible, viscous fluids in the axisymmetric coordinate system were solved using a control volume method. The volume-of-fluid (VOF) technique was used to track the liquid free-surface. The findings of the present study can be summarized as the following:

1) The results of the model were compared and validated with those of the experiments reported in the literature.
2) The dynamic process after impact was found to be sensitive to the initial droplet velocity and the thickness of the liquid film. Non-dimensional maximum crown height and its corresponding time were studied for a range of We numbers. The non-dimensional film thickness had a small effect on the non-dimensional parameters related to the maximum crown height and its corresponding time.
3) The critical We number for splashing (We_{cr}) was studied for Oh (Ohnesorge) numbers in the range of 0.01–0.1. A comparison between the numerical results and experimental measurements showed that the model can accurately predict the critical We number. The numerical model was also used to simulate cases with lower Oh number (Oh~0.001) where no measurements are reported due to the limitations in the experiments.
4) The critical We number was found insensitive to the non-dimensional film thickness; it decreased, however, with decreasing Oh number or liquid viscosity.
5) Using the extensive results of the model, simple expressions were developed that correlate the non-dimensional parameters involved in droplet impingement onto a thin liquid film.

REFERENCES

[1] M. Pasandideh-Fard, S. Chandra, and J. Mostaghimi, "A Three-Dimensional Model of Droplet Impact and Solidification", *Int. J. Heat Mass Trans.*, **45**(2002), p. 2229.

[2] M. Pasandideh-Fard, V. Pershin, S. Chandra, and J. Mostaghimi, "Splat Shapes in a Thermal Spray Coating Process: Simulations and Experiments", *J. Thermal Spray Technology*, **11**(2002), p. 206.

[3] R. Ghafouri-Azar, J. Mostaghimi, and S. Chandra, "Numerical Study of Impact and Solidification of a Droplet over a Deposited Frozen Splat", *Int. J. Comput. Fluid Dyn.*, **18**(2004), p. 133.

[4] H. Fujimoto, Y. Shiotani, A. Y. Tong, T. Hama, and H. Takuda, "Three-Dimensional Numerical Analysis of the Deformation Behavior of Droplets Impinging onto a Solid Substrate", *Int. J. Multiphase Flow*, **33**(2007), p. 317.

[5] P. Walzel, "Zerteilgrenze beim Tropfenaufprall", *Chem. Ing. Tech.* **52**(1980), p. 338.

[6] C. Mundo, M. Sommerfeld, and C. Tropea, "Experimental Studies of the Deposition and Splashing of Small Liquid Droplets Impinging on a Flat Surface", In *Proc. 6th Intl Conf. on Liquid Atomization and Spray Systems,* (1994), Rouen, p. 134.

[7] A. B. Wang and C. C. Chen, "Splashing Impact of a Single Drop onto Very Thin Liquid Films", *Phys. Fluids*, **12**(2000), p. 2155.

[8] G. E. Cossali, M. Marengo, A. Coghe, and S. Zhdanov, "The Role of Time in Single Drop Plash on Thin Film", *Experiments in Fluids*, **36**(2004), p. 888.

[9] F. H. Harlow and J. P. Shannon, "The Splash of a Liquid Droplet", *J. Appl. Phys*., **38**(1967), p. 3855.

[10] G. Trapaga, J. Szekely, "Mathematical Modeling of the Isothermal Impingement of Liquid Droplets in Spraying Processes", *Metall. Trans.*, **B 22**(1991), p. 901.

[11] "FLOW-3D: Computational Modeling Power for Scientists and Engineers", *Technical Report FSI-88-00-1*, Flow Science Inc.,(1988), San Diego, CA.

[12] H. Liu, E. J. Lavernia, and R. Rangel, "Numerical Simulation of Substrate Impact and Freezing of Droplets in Plasma Spray Processes", *J. Phys*., **D 26**(1993), p. 1900.

[13] D. B. Kothe, R. C. Mjolsness, and M. D. Torrey, "RIPPLE: A Computer Program for Incompressible Flows With Free Surfaces", *Technical Report LA-12007-MS*, LANL, Los Alamos, NM, (1991).

[14] M. Pasandideh-Fard, Y. M. Qiao, S. Chandra, and J. Mostaghimi, "Capillary Effects During Droplet Impact on a Solid Surface", *Phys. Fluids*, **8(3)**(1996), p. 650.

[15] C.W. Hirt and B. D. Nichols, "Volume of Fluid (VOF) Methods for the Dynamics of Free Boundaries", *J. Comput. Phys*., **39**(1981), p. 201.

[16] J. Fukai, Y. Shiiba, T. Yamamoto, O. Miyatake, D. Poulikakos, C. M. Megaridis, and Z. Zhao, "Wetting Effects on the Spreading of a Liquid Droplet Colliding With a Flat Surface: Experiment and Modeling", *Phys. Fluids*, **7**(1995), p. 236.

[17] M. Bussman, J. Mostaghimi, and S. Chandra, "On a Three-Dimensional Volume Tracking Model of Droplet Impact", *Phys. Fluids*, **11(6)**(1999), p. 1406.

[18] C. Josserand and S. Zaleski, "Droplet Splashing on a Thin Liquid Film", *Phys. Fluids*, **15(6)**(2003), p. 1650.

[19] H. Xie, S. Koshizuka, and Y. Oka, "Modeling of a Single Drop Impact onto Liquid Film Using Particle Method", *Int. J. Numer. Meth. Fluids*, **45**(2004), p. 1009.

[20] J. Mostaghimi, M. Pasandideh-Fard, and S. Chandra, "Dynamics of Splat Formation in Plasma Spray', *Plasma Chemistry and Plasma Processing*, **22(1)** (2002).

[21] J. U. Brackbill, D. B. Kothe, and C. Zemach, "A Continuum Method for Modeling Surface Tension", *J. Comput. Phys*., **100**(1992), p. 335.

[22] D. L. Youngs, "An Interface Tracking Method for a 3D Eulerian Hydrodynamics Code", *Technical Report 44/92/35*, AWRE, (1984).